J. Marine. Sci. Appl. (2010) 9: 34-41
DOI: 10.1007/s11804-010-8037-9

Numerical Simulation of Dam Breaking Using Smoothed Particle Hydrodynamics and Viscosity Behavior

Xing Zheng* **and Wen-yang Duan**

College of Shipbuilding Engineering, Harbin Engineering University, Harbin 150001, China

Abstract: Smoothed particle hydrodynamics (SPH) is a Lagrangian meshless particle method. It is one of the best method for simulating violent free surface flows in fluids and solving large fluid deformations. Dam breaking is a typical example of these problems. The basis of SPH was reviewed, including some techniques for governing equation resolution, such as the stepping method and the boundary handling method. Then numerical results of a dam breaking simulation were discussed, and the benefits of concepts like artificial viscosity and position correction were analyzed in detail. When compared with dam breaking simulated by the volume of fluid (VOF) method, the wave profile generated by SPH had good agreement, but the pressure had only reasonable agreement. Improving pressure results is clearly an important next step for research.
Keywords: meshless method; smoothed particle hydrodynamics (SPH); dam breaking; free surface flow
Article ID: 1671-9433(2010)01-0034-08

1 Introduction

Violent wave motion is a common phenomenon in marine and coastal engineering. When the wave encounters a structure in its path, very large impact can occur together with wave overturning, breaking and splashing. Current probe into this kind of problem very much depends on laboratory experiment, which can be very expansive, time-consuming or even hazardous. The other important issue is of course the scaling effect. Numerical simulations have also been used for this type of problem (Hu and Kashiwagi, 2004; Chen and Yu, 2009; Koshisuka *et al*., 1998). Although significant progress has been made, the success is still very much limited, especially in the cases where the free surface profile remains smooth (Xu and Duan, 2008; Xu and Duan, 2009). One of the reasons for this is that for the adopted mesh based method it is very difficult to generate a grid of high quality and high resolution for the overturning and breaking waves. This paper investigates the potential of applying a non-mesh based method to the violent free surface.

Smoothed particle hydrodynamics (SPH) method is a meshless technique. It divides the fluid domain into a finite number of mass carrying particles. The movement of the particles and the pressure distribution in the fluid are obtained by solving the momentum equations and continuity equation within the Lagranian description of the motion. The method was first developed to simulate the evolution in astrophysics (Lucy, 1977; Gingold and Monaghan, 1997), and was extended to free surface flow problem by Monaghan (1994). Because the path of each particle is tracked in SPH, the movement of particles can implicitly satisfy the kinematic condition on the free surface (Souto *et al*., 2006). Because it does not require a mesh, it has the potential to deal with the complex free surface flows. Lo and Shao (2002) used SPH method together with a large eddy simulation approach to simulate the offshore solitary wave. Colagrossi and Landrini (2003) applied SPH method to the two-dimensional interfacial flows. Souto *et al*. (2004) calculated the phase lag between the tank motion and the liquid response moment by SPH method. Furthermore sloshing moment amplitudes in a wide range of rolling frequencies were also obtained using SPH by Souto *et al*. (2006).

In the following sections, the authors give a brief description of the mathematical formulation and its numerical solution method. Then behaviours of numerical viscosity of SPH are compared in details, the combined method is recommended for violent free surface flow simulation. At last, numerical results of SPH are given for comparison with VOF method.

2 Foundation of SPH

The foundation of SPH includes kernel approximation and particle approximation. The kernel approximation can be illustrated with the following identity.

$$f(\boldsymbol{x}) = \int_{\Omega} f(\boldsymbol{x}')\delta(\boldsymbol{x}-\boldsymbol{x}')\mathrm{d}\boldsymbol{x}' \tag{1}$$

where δ is the Dirac delta function given by

$$\delta(\boldsymbol{x}-\boldsymbol{x}') = \begin{cases} \infty & \boldsymbol{x}=\boldsymbol{x}' \\ 0 & \boldsymbol{x}\neq\boldsymbol{x}' \end{cases} \tag{2}$$

in Eq.(1), Ω is the influent domain. If the delta function is substituted by smooth function $W(\boldsymbol{x}-\boldsymbol{x}',h)$, the integration

Received date: 2008-06-23.
Foundation item: Supported by the National Natural Science Foundation of China under Grant No. 10572041 and 50779008.
***Corresponding author Email:** zhengxing1106@yahoo.com.cn

representation of Eq.(1) can become

$$f(\boldsymbol{x}) = \int_{\Omega} f(\boldsymbol{x}')W(\boldsymbol{x}-\boldsymbol{x}',h)\mathrm{d}\boldsymbol{x}' \tag{3}$$

where $W(\boldsymbol{x}-\boldsymbol{x}',h)$ is the so-called kernel function, and h is the smooth length. In fact, Eq.(3) can only be an approximation. The kernel function W in Eq.(3) satisfies the following conditions

$$\int_{\Omega} W(\boldsymbol{x}-\boldsymbol{x}',h)\mathrm{d}\boldsymbol{x}' = 1 \tag{4}$$

$$\lim_{h\to 0} W(\boldsymbol{x}-\boldsymbol{x}',h) = \delta(\boldsymbol{x}-\boldsymbol{x}') \tag{5}$$

$$W(\boldsymbol{x}-\boldsymbol{x}',h) = 0 \qquad \left|\boldsymbol{x}-\boldsymbol{x}'\right| \geq kh \tag{6}$$

where k is the coefficient related to the form of the smooth function.

The kernel approximation of spatial derivative $\nabla\cdot f(\boldsymbol{x})$ is obtained simply by substituting $f(\boldsymbol{x})$ with $\nabla\cdot f(\boldsymbol{x})$ in Eq.(3), which gives

$$\nabla\cdot f(\boldsymbol{x}) = \int_{\Omega} \nabla\cdot f(\boldsymbol{x}')W(\boldsymbol{x}-\boldsymbol{x}',h)\mathrm{d}\boldsymbol{x}' \tag{7}$$

where since

$$\begin{aligned}\nabla\cdot f(\boldsymbol{x}')W(\boldsymbol{x}-\boldsymbol{x}',h) = \nabla\cdot[f(\boldsymbol{x}')W(\boldsymbol{x}-\boldsymbol{x}',h)] - \\ f(\boldsymbol{x}')\cdot\nabla W(\boldsymbol{x}-\boldsymbol{x}',h)\end{aligned} \tag{8}$$

substituting to Eq.(7), which gives

$$\begin{aligned}\nabla\cdot f(\boldsymbol{x}) = &\int_{\Omega} \nabla\cdot[f(\boldsymbol{x}')W(\boldsymbol{x}-\boldsymbol{x}',h)]\mathrm{d}\boldsymbol{x}' - \\ &\int_{\Omega} f(\boldsymbol{x}')\cdot\nabla W(\boldsymbol{x}-\boldsymbol{x}',h)\mathrm{d}\boldsymbol{x}' = \\ &\int_{S} [f(\boldsymbol{x}')W(\boldsymbol{x}-\boldsymbol{x}',h)\boldsymbol{n}\mathrm{d}S - \\ &\int_{\Omega} f(\boldsymbol{x}')\cdot\nabla W(\boldsymbol{x}-\boldsymbol{x}',h)\mathrm{d}\boldsymbol{x}'\end{aligned} \tag{9}$$

where $\boldsymbol{n}$ is the unit vector normal to the surface S. Since the smooth function W is defined to have compact support, and the surface integral on the right-hand side of Eq.(9) is zero. In this paper, cubic spline kernel function is adopted for the simulation, which has the same form used by Monaghan (1994). Therefore, Eq.(9) is simplified as follows:

$$\nabla\cdot f(\boldsymbol{x}) = -\int_{\Omega} f(\boldsymbol{x}')\cdot\nabla W(\boldsymbol{x}-\boldsymbol{x}',h)\mathrm{d}\boldsymbol{x}' \tag{10}$$

where change the coordinate of ∇W from $\boldsymbol{x}'$ to $\boldsymbol{x}$, a minus signal appears:

$$\nabla_{\boldsymbol{x}'} W = -\nabla_{\boldsymbol{x}} W \tag{11}$$

substituting Eq.(11) to Eq.(10), this is the form of spatial derivative widely used:

$$\nabla\cdot f(\boldsymbol{x}) = \int_{\Omega} f(\boldsymbol{x}')\cdot\nabla_{\boldsymbol{x}} W(\boldsymbol{x}-\boldsymbol{x}',h)\mathrm{d}\boldsymbol{x}' \tag{12}$$

The subscript $\boldsymbol{x}$ usually can be omitted during the expression of spatial derivative.

When the computing domain is discretized to a mass of particles, each particle j takes mass m_j and density ρ_j, the volume of each particle can be obtained by m_j/ρ_j. So the discretized form of Eq.(7) and Eq.(12) are given as follows:

$$f(\boldsymbol{x}_i) = \sum_{j=1}^{N} \frac{m_j}{\rho_j} f(\boldsymbol{x}_j)W(\boldsymbol{x}_i-\boldsymbol{x}_j,h) \tag{13}$$

$$\nabla f(\boldsymbol{x}_j) = \sum_{j=1}^{N} \frac{m_j}{\rho_j} f(\boldsymbol{x}_j)\nabla W(\boldsymbol{x}_i-\boldsymbol{x}_j,h) \tag{14}$$

which are the form of particle approximation.

For water flow problem, the governing equations should include the mass conservation equation, which gives

$$\frac{\mathrm{D}\rho}{\mathrm{D}t} = -\rho\nabla\cdot\boldsymbol{V} \tag{15}$$

where

$$\frac{\mathrm{D}\rho_i}{\mathrm{D}t} = -\rho_i\sum_{j=1}^{N}\frac{m_j}{\rho_j}\boldsymbol{V}_j\cdot\nabla W_{ij} \tag{16}$$

Symmetry property of ∇W_{ij} can get $\sum_{j=1}^{N}\nabla W_{ij} = 0$, and the following equation exists

$$\begin{aligned}-\sum_{j=1}^{N}\frac{m_j}{\rho_j}\boldsymbol{V}_j\cdot\nabla W_{ij} = -\sum_{j=1}^{N}\frac{m_j}{\rho_j}\boldsymbol{V}_j\nabla\cdot W_{ij} + \\ \boldsymbol{V}_i\cdot\sum_{j=1}^{N}\frac{m_j}{\rho_j}\nabla W_{ij} = \sum_{j=1}^{N}\frac{m_j}{\rho_j}\boldsymbol{V}_{ij}\cdot\nabla W_{ij}\end{aligned} \tag{17}$$

Substituting Eq.(17) to Eq.(16) can get

$$\frac{\mathrm{D}\rho_i}{\mathrm{D}t} = \rho_i\sum_{j=1}^{N}\frac{m_j}{\rho_j}\boldsymbol{V}_{ij}\cdot\nabla W_{ij} \tag{18}$$

where $V_{ij} = V_i - V_j$. Note that various ways exist to express gradients in continuous form, i.e.

$$\nabla f = \rho[\nabla(\frac{f}{\rho}) + \frac{f}{\rho^2}\nabla\rho] \tag{19}$$

which leads to different discrete SPH forms. Combining Eqs.(14) and (19) gives the following SPH form:

$$\nabla f = \rho_i\sum_{j=1}^{N} m_j(\frac{f_i}{\rho_i^2} + \frac{f_j}{\rho_j^2})\nabla W_{ij} \tag{20}$$

This form ensures linear momentum conservation and is used for pressure gradient:

$$\nabla P_i = \rho_i \sum_{j=1}^{N} m_j \left(\frac{P_i}{\rho_i^2} + \frac{P_j}{\rho_j^2}\right) \nabla W_{ij} \tag{21}$$

This is the expression of pressure term in the momentum conservation. But the viscosity term has different forms. Previous expressions used to calculate realistic viscous force have typically involved nested summations over the particles, or have directly employed second derivatives of the kernel (Takeda *et al*., 1994). The disadvantage of using second derivatives is that interpolation is much more susceptible to error at low resolution, especially for low-order spline kernels. Most implementations of SPH employ an artificial viscosity first introduced to permit the modelling of strong shocks and free surface flow. This viscosity gets the form

$$\Pi_{ij} = \begin{cases} \dfrac{-\alpha \bar{c}_{ij} \phi_{ij}}{\bar{\rho}_{ij}} & \boldsymbol{v}_{ij} \cdot \boldsymbol{x}_{ij} < 0 \\ 0 & \boldsymbol{v}_{ij} \cdot \boldsymbol{x}_{ij} \geq 0 \end{cases} \tag{22}$$

where $\phi_{ij} = h_{ij} \boldsymbol{v}_{ij} \cdot \boldsymbol{x}_{ij} / \left(\left|\boldsymbol{x}_{ij}\right|^2 + 0.01 h_{ij}^2\right)$, $\bar{c}_{ij} = \dfrac{c_j + c_j}{2}$, $\bar{\rho}_{ij} = \dfrac{\rho_i + \rho_j}{2}$, $h_{ij} = \dfrac{h_i + h_j}{2}$, $\boldsymbol{v}_{ij} = \boldsymbol{v}_i - \boldsymbol{v}_j$, $\boldsymbol{x}_{ij} = \boldsymbol{x}_i - \boldsymbol{x}_j$. This viscosity term is incorporated into the momentum equation

$$\frac{\mathrm{D}V^{\alpha}}{\mathrm{D}t} = -\sum_{j=1}^{N} m_j \left(\frac{P_i}{\rho_i^2} + \frac{P_j}{\rho_j^2} + \Pi_{ij}\right) \nabla^{\alpha} W_{ij} + F_i^{\alpha} \tag{23}$$

F_i^{α} is the external volume force such as gravity in wave simulation.

3 Numerical schemes

3.1 Stepping method

This method is fully explicit in time. The following equations give the sequence of the algorithm.

$$\boldsymbol{u}_{n+1} = \boldsymbol{u}_n + \left(-\frac{1}{\rho} \nabla P_n + \Pi_n + \boldsymbol{F}_i\right) \Delta t \tag{24}$$

where subscripts *n* and *n*+1 indicate the present and next time steps respectively. Δt is the time step length. Density is updated at the next time step by

$$\rho_{n+1} = \rho_{n+1} - \rho_{n+1} (\nabla \cdot \boldsymbol{u}_{n+1}) \Delta t \tag{25}$$

There makes an assumption that pressure and density can get explicit relation (Monaghan, 1994), which exists

$$P = P_0 \left[\left(\frac{\rho}{\rho_0}\right)^{\gamma} - 1\right] \tag{26}$$

where $P_0 = C_0^2 \rho_0 / \gamma$, and C_0 is the artificial sound speed. In the following calculations, γ=7 is taken and when the fluid is water, C_0 is taken as ten times the maximum velocity. So the pressure at present step is obtained by

$$P_{n+1} = P_0 \left[\left(\frac{\rho_{n+1}}{\rho_0}\right)^{\gamma} - 1\right] \tag{27}$$

The position is updated at the next step by

$$\boldsymbol{r}_{n+1} = \boldsymbol{r}_n + \boldsymbol{u}_{n+1} \Delta t \tag{28}$$

The position is very sensitive to the density and pressure. In this paper, two terms are added to improve the calculation stability. The first term is acceleration, which can be considered as the second order derivative of position, the second one is the position correction (Monaghan, 1994), which will prevent the particle penetration and treat particle disorder arrangement. Eq.(28) can be improved by

$$\boldsymbol{r}_{n+1} = \boldsymbol{r}_n + (\boldsymbol{u}_{n+1} - \varepsilon \sum_{j}^{N} \frac{m_j}{\rho_j} \boldsymbol{V}_{ij} W_{ij}) \Delta t + \frac{1}{2} \mathrm{d}\boldsymbol{u}_{n+1} \Delta t^2 \tag{29}$$

where ε is a constant coefficient which is usually chosen between 0 and 1, and $\mathrm{d}\boldsymbol{u}_{n+1}$ is the acceleration of the next step, which can use present step for easy.

$$\mathrm{d}\boldsymbol{u}_{n+1} = -\frac{1}{\rho} \nabla P_n + \Pi_n + \boldsymbol{F}_i \tag{30}$$

The total time integration uses improved Euler method.

3.2 Boundary condition

3.2.1 Wall boundary

Water flows in this paper have two types of boundary, i.e. wall boundary and free surface boundary. For wall boundary, zero velocity of vertical direction on the wall and density re-injected of outside wall need to be satisfied. For free surface treatment, the pressure is automatically obtained by the knowledge of density, but surface particle tracking is also needed for result comparison.

There are several ways to handle the wall boundary, i.e. repulsive forces (Monaghan, 1992) and ghost particles (Takeda *et al*., 1994; Morris, 1997). With repulsive forces, only one layer of particles is placed on the wall, they exert very large repulsive forces to prevent fluid particles from crossing the walls. Density scarcity and repulsive force make the particle oscillation near the boundary. Ghost particles are used here. They are distributed outside the wall. Some information, like position, velocity and pressure are located as follows:

$$x_g = 2x_w - x_i \tag{31}$$

$$y_g = 2y_w - y_i \tag{32}$$

$$u_g = 2u_w - u_i \tag{33}$$

$$v_g = 2v_w - v_i \tag{34}$$

$$P_g = P_i \tag{35}$$

where subscript i is the free particle, g is the ghost particle, and w is corresponding wall. In this paper, only outside corner is used. Fig.1 illustrates the relationship of ghost particles near the corner. There are two steps for ghost particle arrangement, namely, locate the ghost particles in horizontal direction firstly, then according to the vertical wall get the ghost particles in vertical direction.

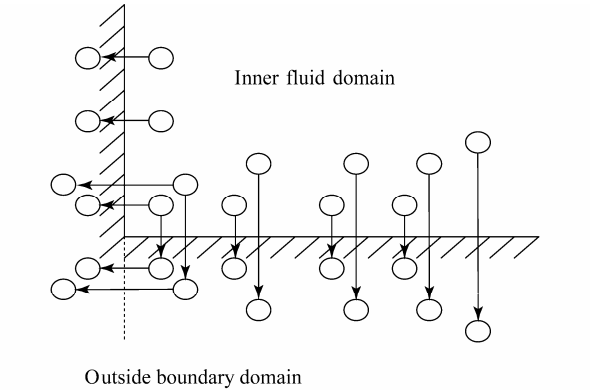

Fig.1 Sketch of ghost particle arrangement near the corner

3.2.2 Free surface particle tracking

No ghost particle is used to set the free surface boundary conditions. But it is necessary to track the free surface particles. For 2-D simulations, the ratio between neighbour particles and influence domain determines whether the particle is inner fluid particle or free surface particle

$$f_i = \sum_{j=1}^{N} V_j / [\pi(\kappa h_i)^2] \tag{36}$$

where V_j is the space of each neighbour particle, κ is the coefficient according to the form of kernel functions, for cubic spline kernel κ=2. Hence, a criterion set to $f_i \le 0.75$ is used to determine which particles belong to the free surface. Fig.2 shows the results of the method for free surface particle tracking.

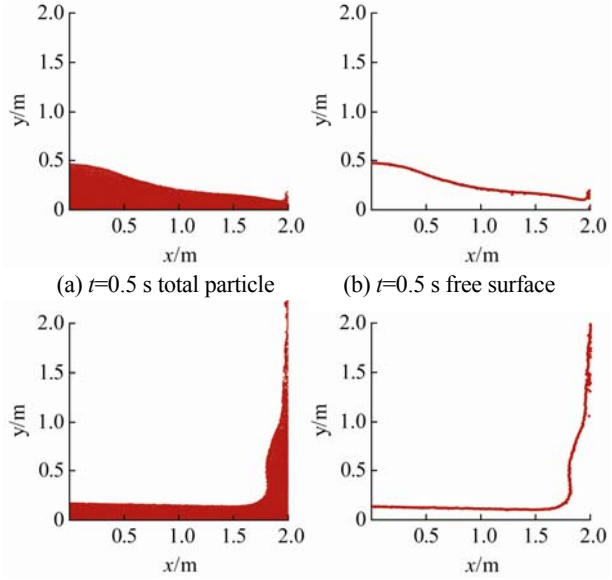

(a) t=0.5 s total particle (b) t=0.5 s free surface

(c) t=1.0 s total particle (d) t=1.0 s free surface

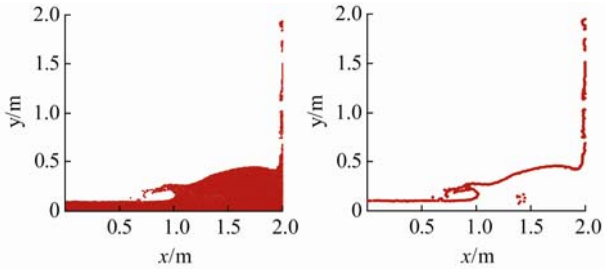

(e) t=1.5 s total particle (f) t=1.5 s free surface

Fig.2 Results of free surface particle tracking

4 Numerical results

In this section, SPH method is used for dam breaking simulation. Although this numerical model is not a new attempt for SPH, the purpose of this simulation is to get the behaviors of artificial viscosity and position correction, which play the same role in preventing particle penetration and keeping particles order arrangement. The combination of two methods will improve stability and reliability of the results. Configuration of dam breaking is shown in Fig.3. There is a rectangular water volume at initial time. Total fluid particle is 800, and kernel function adopts cubic spline, time step Δt =0.000 1 s.

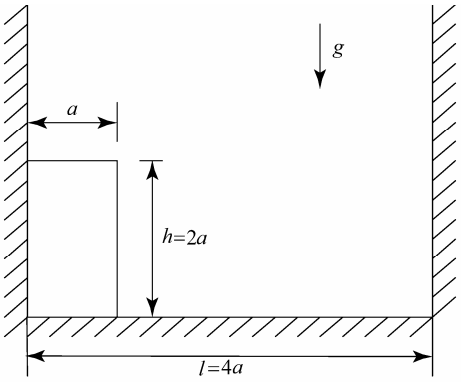

Fig.3 Configuration of dam breaking on dry bed

4.1 Artificial viscosity effects

This part will introduce the single role of position correction. The coefficient of α in Eq.(22) takes 0.01 firstly. The total process of dam breaking stops at 1.5 s. Profiles of dam breaking are shown in Fig.4. Before wave front hits the right vertical wall, free surface profile is smooth. No divergent phenomenon happens in local area. After wave front hit the vertical wall, wave elevation rises fast, free surface becomes splashing, and local area near left wall corner diverges suddenly after 1.5 s. When α=0.06, after wave front hit the vertical wall, the speed of discrete particle decreases; after t=1.5 s, the whole system is still stable, as shown in Fig.5. According to the tests, artificial viscosity is important for the simulation. When α is small, the profile surface is smoothed at the beginning. After the wave front hit the vertical wave, splashing is violent and some particles of very high speed will make the whole particle system unsteady. When α increases, the free surface can become more

smoothed and the whole system is convergent. So if the total process is reliable, the coefficient α should take a value big enough. In this case, $\alpha \geq 0.06$. If ε is too large, it will make more numerical viscosity. This paper accommodates α=0.06~0.15 for dam breaking simulation.

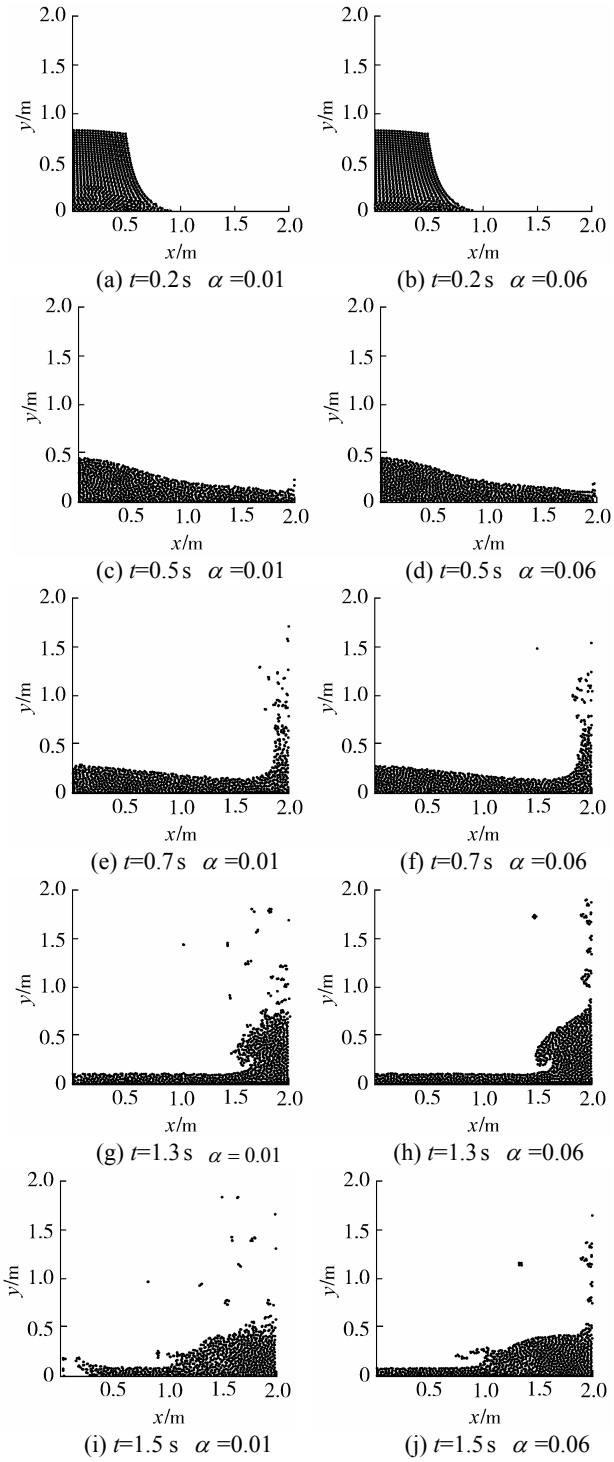

(a) t=0.2 s α=0.01 (b) t=0.2 s α=0.06
(c) t=0.5 s α=0.01 (d) t=0.5 s α=0.06
(e) t=0.7 s α=0.01 (f) t=0.7 s α=0.06
(g) t=1.3 s α=0.01 (h) t=1.3 s α=0.06
(i) t=1.5 s α=0.01 (j) t=1.5 s α=0.06

Fig.4 Process of dam breaking at different time

4.2 Position correction effect

This part neglects the effect of viscosity and only considers the position correction in Eq.(29). Taking the same step as the last section, and it is found when $\varepsilon = 0.03$, the total system becomes convergent. Comparison of two cases is shown in Fig.5, where Solid Square shows the results of position correction, $\varepsilon = 0.03$, and cored circle is the result of artificial viscosity, α=0.06. According to the comparison, there is a little difference when wave front is not overturning. When the over-turning appears, e.g. at t=1.3 s, there are some differences between two methods. Position correction makes the over-turning and splashing smoothed and artificial viscosity can keep free surface active and vigorous after over-turning.

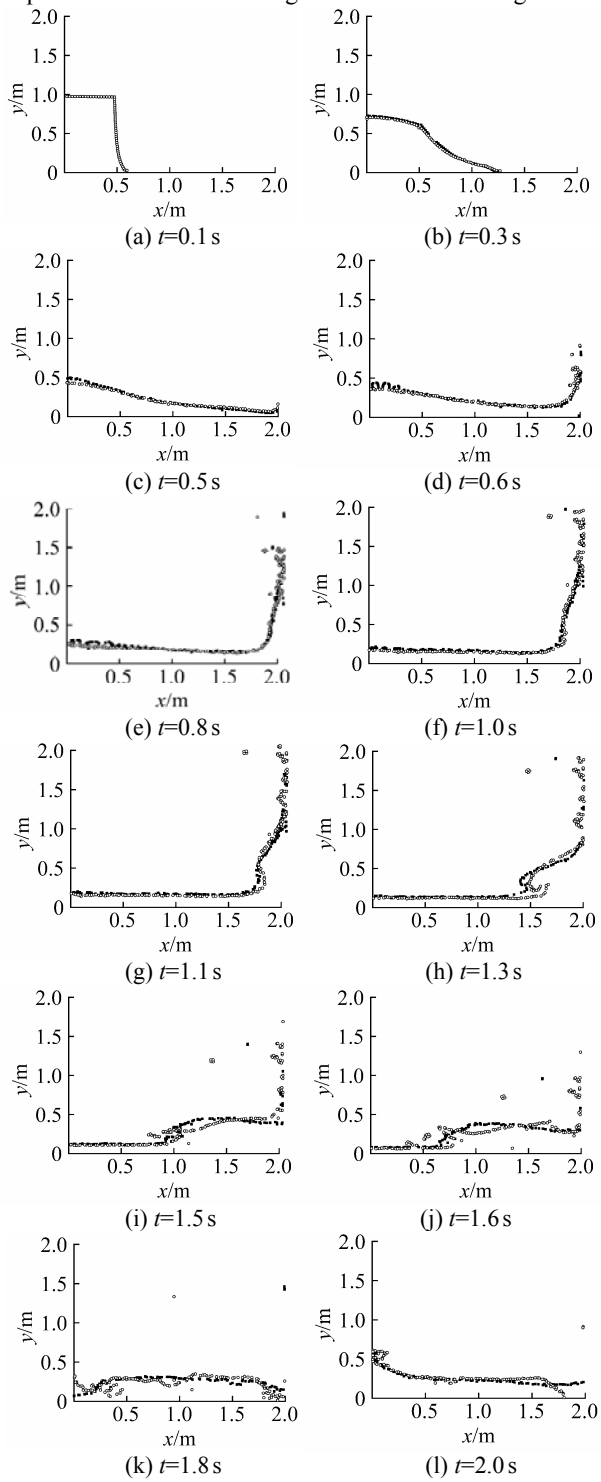

(a) t=0.1 s (b) t=0.3 s
(c) t=0.5 s (d) t=0.6 s
(e) t=0.8 s (f) t=1.0 s
(g) t=1.1 s (h) t=1.3 s
(i) t=1.5 s (j) t=1.6 s
(k) t=1.8 s (l) t=2.0 s

Fig.5 Comparison of different methods for dambreaking at different times

4.3 Combination of two methods

Two techniques for viscosity handling are combined for dam breaking simulation in this section. On the one hand, position correction makes the whole particle steady enough; on the other hand, artificial viscosity can decrease numerical viscosity and get better agreement with realistic condition. The number of particles in fluid domain is 5 000, $\varepsilon = 0.03$ and α =0.06. The results of wave profile can be shown in Fig.6.

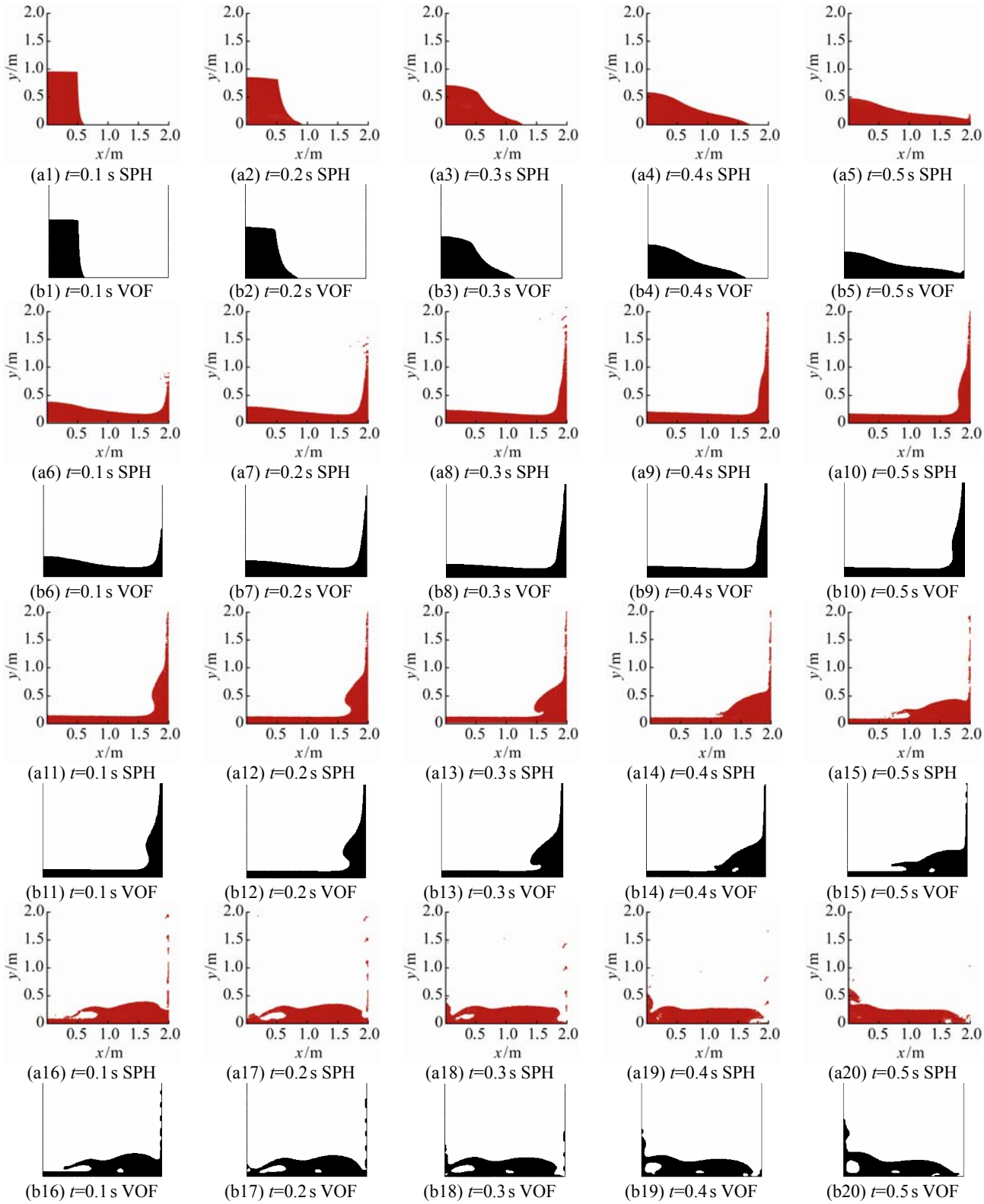

Fig.6 Comparison of dam breaking process

The average density $\bar{\rho}$ of total fluid particles is a criterion for stability and mass conservation. The process of $\bar{\rho}$ is shown in Fig.7. $\bar{\rho}$ has very small change during the simulation, $\Delta\bar{\rho}/\bar{\rho} \le 0.3\%$. Total energy of the whole particle system can be defined as

$$E_t = E_p + E_v = \sum_{j=1}^{N} m_j g H_i + \frac{1}{2}\sum_{j=1}^{N} m_j V_j^2 \tag{37}$$

where E_p is the total potential energy, E_v the total kinetic energy, m_j the mass of each particle, H_i the height above the dry bottom, V_j the velocity of each particle, and N the total number of particles. The process of the total energy variety is shown in Fig.8. The total energy is decreased during the whole process because of viscous dissipation. When velocity increases, the total energy decreases faster when t=0.5~2.0 s. When velocity is small, the total energy declines slowly.

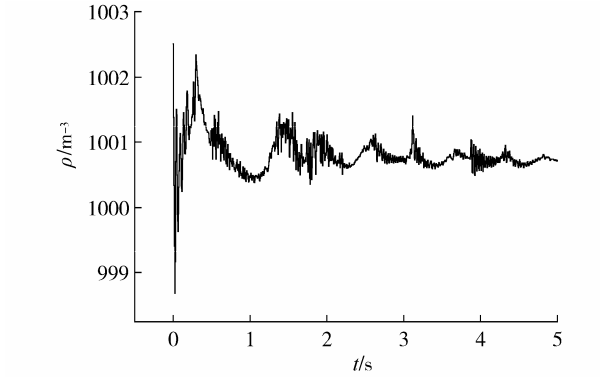

Fig.7 Process of $\bar{\rho}$ variety during the simulation

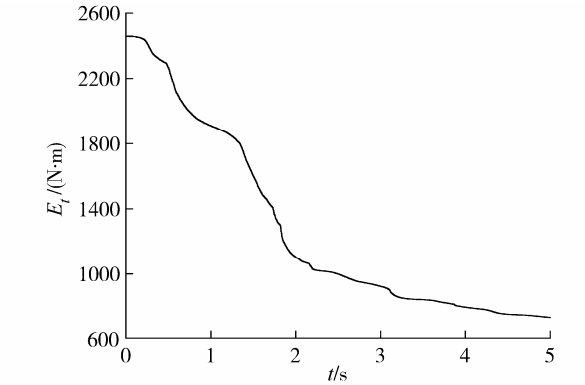

Fig.8 Process of the total energy variety during the simulation

4.4 Pressure on vertical wall

The pressure on the right vertical wall is checked by $F_t = \int_l P\mathrm{d}l$, F_t is the pressure integral of the right vertical wall, P is the total pressure near right vertical wall, l is the wet distance between fluid and vertical wall being contacted. Fig.9 is pressure integral of the left wall during the whole process by VOF method and SPH method. According to the comparison, the tendency of two methods is similar to the pressure integral. SPH exists violent oscillating during the process. The reason is of explicit relationship between density and pressure. Very small density variety can generate very big pressure results, it is necessary to do more research in refining the process of pressure, remaining the useful information and deleting the pseudo signals.

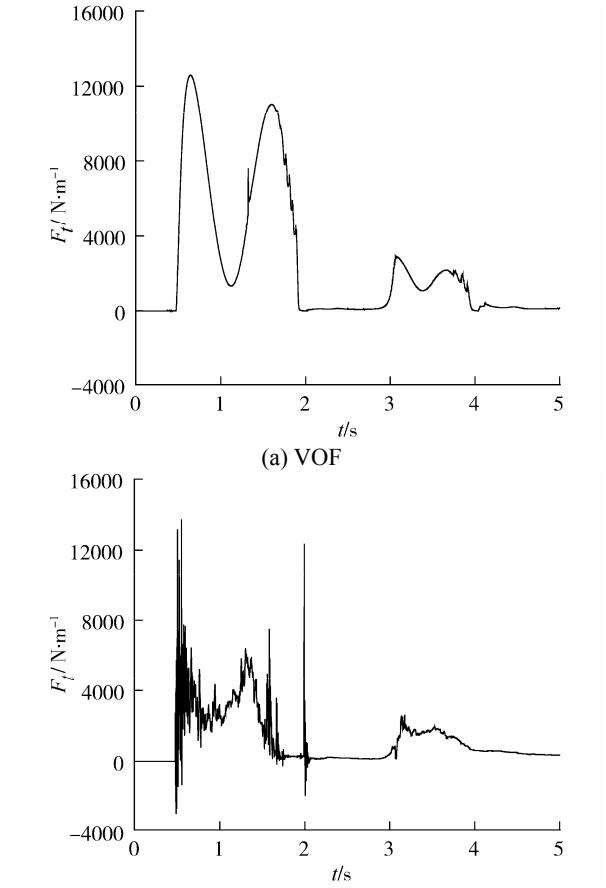

Fig.9 Process of total pressure integral

5 Conclusions and remarks

The implementation of SPH method is introduced to simulate dam breaking problems. Two numerical techniques, i.e. artificial viscosity and position correction, are investigated in details. Two methods can get agreeable results when the free surface is kept smoothed. When the wave front hits the vertical wall, the differences become obvious with the process going on. The proposed form of combining two methods can make the algorithm stable and high in resolution. From the comparison of VOF, two methods can get a good agreement at most time. When over-turning and re-entering occur, SPH can not catch the process of cavitation bubble accurately because of the one-phase

model. Total pressure integral of the right vertical wall is compared by two methods. The variety tendency is similar but the small-scale oscillation still exists. It needs more research on the basic algorithm to filter out the pressure oscillations. SPH method is a robust meshless particle method. Its powerful and vigorous advantages need more investigation on the high accuracy algorithm and mature numerical techniques. It still has a long way to improve present SPH method.

References

Colagrossi A, Landrini M (2003). Numerical simulation of interfacial flow by smoothed particle hydrodynamics. *Journal of Computational Physics*, **191**(2), 448-475.

Chen HC, Yu K (2009). CFD simulations of wave-current-body interactions including greenwater and wet deck slamming. *Computer & Fluids*, **38**(5), 970-980.

Gingold RA, Monaghan JJ (1977). Smoothed particle hydrodynamics: theory and applications to non-spherical stars. *Mon Not Roy Astrou Soc*, **181**, 375-389.

Hu CH, Kashiwagi M (2004). A CIP-based method for numerical simulations of violent free-surface flows. *Journal of Marine Science and Technology*, **9**(4), 143-157.

Koshizuka S, Nobe A, Oka Y (1998). Numerical analysis of breaking waves using the moving particle semi-implicit method. *International Journal for Numerical Methods in Fluids*, **26**(7), 751-769.

Lucy LB (1977). A numerical approach to the testing of the fission hypothesis. *The Astronomical Journal*, **8**(12), 1013- 1024.

Lo EYM, Shao SD (2002). Simulation of near-shore solitary wave mechanics by an incompressible SPH method. *Applied Ocean Research*, **24**(5), 275-286.

Monaghan JJ (1992). Smoothed Particle Hydrodynamics. *Annual Review Astronomy & Astro-physics*, **30**, 543-574.

Monaghan JJ (1994). Simulating free surface flows with SPH. *Journal of Computational Physics*, **110**(2), 399-406.

Morris JP (1997). Modeling low Reynolds number incompressible flow using SPH. *Journal of Computational Physics*, **136**(1), 214-226.

Souto IA, Perez RL, Zamora RR (2004). Simulation of anti-roll tanks and sloshing type problems with smoothed particle hydrodynamics. *Ocean Engineering*, **31**(8-9), 1169-1192.

Souto IA, Delorme L, Perez RL, Abril PS (2006). Liquid moment amplitude assessment in sloshing type problems with smooth paritcle hydrodynamics. *Ocean Eengineering*, **33**(11-12), 1462-1484.

Takeda H, Miyama SM, Sekiya M (1994). Numerical simulation of viscous flow by smoothed particle hydrodynamics. *Progress of Theoretical Physics*, **92**(5), 939-960.

Xu Gang, Duan Wenyang (2008). Time domain simulation for water wave radiation by floating structures. *Journal of Marine Science of Application*, **7**(4), 226-235.

Xu Guodong, Duan Wenyang (2009). Review of prediction techniques on hydrodynamic impact of ships. *Journal of Marine Science of Application*, **8**(3), 204-210.

Xing Zheng was born in 1980. He is a doctor at Harbin Engineering University. His current research interests include meshless computation method and hydrodynamics.

Wen-yang Duan was born in 1967. He is a professor at Harbin Engineering University. His current research interests include marine hydrodynamics, time domain BEM, meshless particle methods.